Received 13 July 2016; accepted 14 August 2016. Date of publication 24 August 2016; date of current version 24 October 2016.
The review of this paper was arranged by Editor T.-L. Ren.

Digital Object Identifier 10.1109/JEDS.2016.2602261

On the Small-Signal Capacitance of RF MEMS Switches at Very Low Frequencies

JIAHUI WANG[1] (Student Member, IEEE), JEROEN BIELEN[2], CORA SALM[1] (Senior Member, IEEE), GIJS KRIJNEN[1], AND JURRIAAN SCHMITZ[1] (Senior Member, IEEE)

1 MESA+ Institute for Nanotechnology, University of Twente, 7500 AE Enschede, The Netherlands
2 EPCOS Netherlands B.V., 6525EC Nijmegen, The Netherlands

CORRESPONDING AUTHOR: J. SCHMITZ (e-mail: j.schmitz@utwente.nl)

ABSTRACT This paper presents on-wafer capacitance measurements of silicon-based RF MEMS capacitive switches down to frequencies below 1 Hz. The capacitance-voltage (*C-V*) curve measured at very-low frequency (0.01–10 Hz) deviates from the commonly measured and well-understood high-frequency *C-V* curve, especially near the pull-in and pull-out voltages. This behavior is explained from the mechanical action of the top electrode. An electrostatic transducer model is used to express the coupling between mechanical and electrical behavior of the device under study. The mechanical action and air damping play an important role at the lower measurement frequencies, as confirmed by vibrometer measurements, FEM modeling and experiments at reduced pressure.

INDEX TERMS MEMS, electrical characterization, wafer level testing, RF MEMS switches, capacitive switches, frequency dispersion, capacitance-voltage measurement, very low frequency.

I. INTRODUCTION

RF MEMS capacitive switches are two-terminal devices, with a small-signal capacitance determined by the applied DC voltage [1]–[3]. These switches exhibit very little power consumption, high isolation, low insertion loss and excellent linearity. They have the potential of low cost mass manufacturing and monolithic integration with other electronics [4]. At present they are considered promising candidates for satellite applications, low-noise low-power circuits, portable wireless systems and phased arrays [2], [4].

The capacitance-voltage (*C-V*) measurement is the most commonly used technique to obtain the main electrical parameters of RF MEMS switches [1], [5]. In the scientific literature on these devices, all *C-V* measurements reported to date are conducted at frequencies above 1 kHz [5]–[9]. However, a comprehensive understanding of the devices from DC to RF is necessary for accurate modeling in applications, because this type of switch is often used to process a signal with a very broad spectrum, e.g., in the front end of a wireless receiver.

We have found significant deviations from the commonly observed *C-V* curves when we measure the small-signal capacitance of RF MEMS switches at low frequency (LF), that is, in the 0.01-10 Hz range [10]. For this purpose, we employed a recently developed "very low frequency" measurement technique as well as quasi-static *C-V* measurements. This paper brings new experimental results and an explanation for the differences between the low and high frequency capacitance of the switches. The explanation is based on a one-dimensional analytical model and supported by a three-dimensional FEM model.

II. EXPERIMENTAL

The studied capacitive MEMS switches (Figure 1) are fabricated on a high-resistive 200-mm Si wafer. The movable top electrode, which is the large perforated square (300×300 μm^2) in Figure 1 (a), is an Al membrane suspended by four springs over the Al bottom electrode. The width, length and thickness of each spring are 30 μm, 330 μm and 5 μm respectively. A dielectric layer (SiN_x/SiO_y) is deposited on the bottom electrode. The signal bond pad is connected to the bottom electrode. The top electrode is connected to the two ground bond pads.

The device under test (DUT) is contacted with two micromanipulators in a probe station equipped with

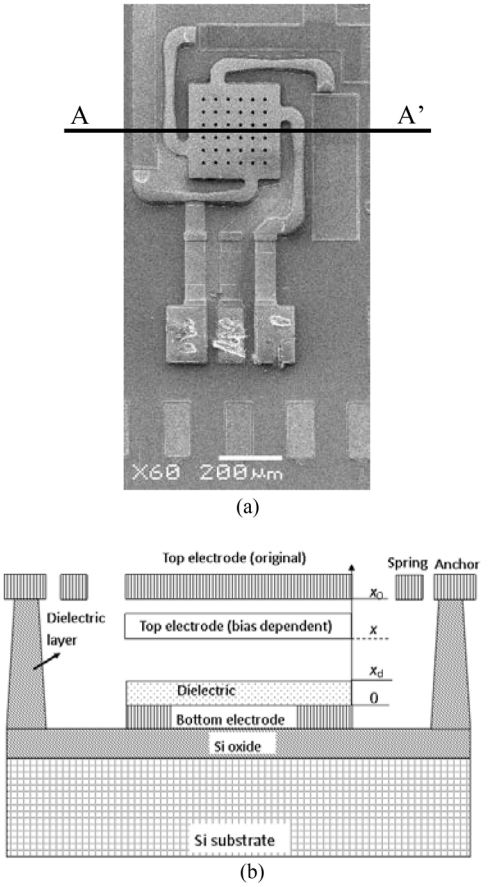

FIGURE 1. (a) top view SEM image of the capacitive MEMS switch; (b) schematic cross section of A-A' in (a). The position of the upper surface of the bottom electrode is defined as height 0; the original height of the top electrode x_0 is 3 µm; the thickness of the dielectric layer x_d is 560 nm; x is the bias dependent height of the top electrode.

a thermochuck. A Keithley SCS 4200 is used for the high frequency (HF) *C-V* measurements typically from 100 kHz to 1 MHz. The same system newly offers the possibility to conduct LF *C-V* measurements in the 0.01-10 Hz range. To this purpose we install two standard pre-amplifiers (Model 4200-PA) on the back panel [11]. All reported measurements are obtained with 80 mV rms AC voltage and 0.1 V step in the DC bias sweep. Quasi-static (QS) and radio-frequency (RF) (100 MHz to 1 GHz) *C-V* measurements are conducted using a Keithley 595 quasi-static meter and a ZVB20 network analyzer, respectively. An MSA-400 Micro System Analyzer is used for the Laser Doppler vibrometer measurements. All measurements are conducted at room temperature and in atmospheric pressure unless specifically mentioned. The devices are not packaged. Hence a preparation process is needed to remove the moisture. This preparation process and the calibration and de-embedding procedures are treated in [10].

III. MEASUREMENTS

The de-embedded *C-V* curves of the RF MEMS capacitive switch (DUT) are shown in Figure 2. The DC bias is swept from 0 V to -30 V, then is swept back to 0 V (the sweep direction is indicated with arrows). At the highest frequencies (black and blue curves), we see the classical *C-V* curve with hysteresis of a capacitive RF MEMS switch: the up-state DUT turns to the down-state at the negative pull-in voltage (V_{pi}), then turns back to the up-state at the negative pull-out voltage (V_{po}). At positive bias, the device exhibits the same behavior. This "classical behavior" is well documented in, e.g., [2], [3], [5] and in the present article, we will focus on the differences between this behavior and the capacitance measured at lower frequencies.

A closer inspection of figure 2 reveals various frequency-dependent features. In the downstate (high capacitance of 5-6 pF) a slight offset is visible between the HF and RF curves, as discussed in Section V. We further see some spikes as marked with oval circles, in the QS and LF *C-V* curves. The prominent spikes in the QS curve occur at the two points of mechanical switching (pull-in and pull-out). Here, the capacitance abruptly changes. To maintain approximately the same voltage, an extra current must be supplied. This is well captured by a quasi-static measurement which measures current continuously. (In the QS measurement, any current is converted to capacitance.) The smaller spike in the LF curve at -15 V is a measurement artefact [10]. The spikes at pull-in and pull-out in the LF curve are sometimes present with varying significance, and are usually smaller than the spikes in the QS curve, as explained in Section IV. As these spikes are transient, and the LF curve is produced by sampling at intervals, measurement timing details determine the appearance of such spikes.

On the upper right side of the graph, we see a gradually growing discrepancy between the HF and RF capacitance on one hand, and the QS and LF capacitance on the other, as marked with a rectangular box. Compared with HF and RF measurements, the QS and LF measurements show a significantly larger capacitance between V_{pi} and V_{po}, namely, 200% larger around V_{pi} and 25% larger around V_{po}. Further, we found that near V_{po} the down-state LF *C-V* curve varies a lot from device to device as shown in figure 3 (a), whereas all other measurements reproduce very well. In some cases, the down-state capacitance increases significantly when the DC bias approaches the pull-out voltage.

In the upstate, with a device capacitance below 1 pF, we see that all measurement techniques yield the same capacitance, except for the region where the device approaches pull-in (also marked with a rectangle in figure 2). A measurement on six different devices on the same wafer, with the same design, gives very comparable results (figure 3 (b)). We will discuss this up-state capacitance difference in Section IV.

To verify if the observed differences between QS and LF on one hand, and HF and RF on the other, are caused by the chosen experimental conditions, a range of sanity checks is performed. We find the same *C-V* behavior on various switches, with various measurement set-ups, and under a wide variety of measurement settings [10]. The LF

C-V curve exhibits a similar shape to the one shown in Figure 2 with an applied frequency from 0.01 Hz to 10 Hz and with an applied rms AC voltage from 20 mV to 500 mV. (This indicates that our small-signal assumption is valid; it should be noted that large signal biasing of this device would require a separate treatment.) It further overlaps with QS *C-V* measurements, independent of the QS sweep rate.

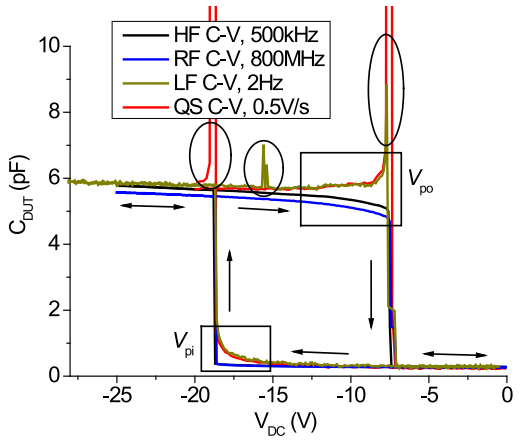

FIGURE 2. Comparison between quasi-static, low-frequency, high-frequency and RF *C-V* curves of an RF MEMS capacitive switch.

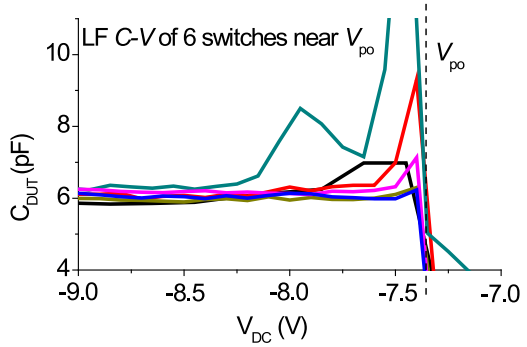

(a)

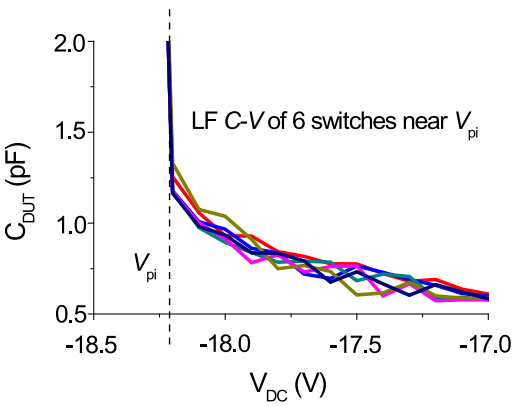

(b)

FIGURE 3. (a) down-state LF *C-V* curves near V_{pi}, measured on 6 equally designed devices on the same wafer; and (b) up-state LF *C-V* curves near V_{po} from the same 6 devices.

The HF *C-V* curve is not influenced by delay times of the DC bias sweep up to 4 s between consecutive measurements in the DC voltage sweep, excluding relaxation effects as a possible explanation of the differences. Environmental humidity does not affect the LF *C-V* curve. No measurement-induced changes have been observed either. These control measurements indicate that the observed frequency dependence of the small-signal capacitances stems from the device itself.

IV. UP-STATE CAPACITANCE

The MEMS switch can be considered a voltage controlled electrostatic transducer. If a voltage change is slow enough for a mechanical reaction, the device finds equilibrium at the lowest internal energy (U), i.e., the sum of capacitive and mechanical (spring) energy; and may move with the changing voltage.

For the up-state, one can derive an equation to describe the impedance of the switch, assuming a one-dimensional system with a mass-loaded spring with spring constant K, moving electrode mass m, and damping characterized by a viscous damping factor α. This damping is predominantly caused by squeeze film damping from the air layer between top and bottom electrode that is squeezed out laterally to the holes and sides of this top electrode. The parallel-plate capacitance is given by

$$C_p = \frac{\varepsilon_0 A_p}{x_e} \tag{1}$$

With x_e the equivalent distance of the top electrode to the bottom electrode (see also figure 1 (b)):

$$x_e = x - x_d + x_d/\varepsilon_r \tag{2}$$

In these equations, A_p is the parallel-plate capacitor area; ε_0 the permittivity in vacuum, and ε_r the relative permittivity of the SiN_x/SiO_y dielectric.

The internal energy of the transducer and its partial differential are given by:

$$U = \frac{V_{DC}^2 \varepsilon_0 A}{2x_e} + \frac{1}{2}K(x - x_0)^2 \tag{3}$$

$$dU = V_{DC}dq + F_{ext}dx \tag{4}$$

Here, V_{DC} is the potential difference between the plates, F_{ext} is the external net force and q is the charge stored in the transducer. The Legendre transform U' can be used to calculate F_{ext} and q, in the present case of a voltage controlled electrostatic transducer [12]. U' and its partial differential are given by:

$$U' = U - qV_{DC} \tag{5}$$

$$dU' = F_{ext}dx - qdV_{DC} \tag{6}$$

F_{ext} and q are calculated from the partial differential of the Legendre transform:

$$F_{ext} = \left(\frac{dU'}{dx}\right) = \frac{V_{DC}^2 \varepsilon_0 A}{2x_e^2} + K(x - x_0) \tag{7}$$

$$q = -\left(\frac{dU'}{dV_{DC}}\right) = \frac{\varepsilon_0 A V_{DC}}{x_e} \tag{8}$$

The differential equations of F_{ext} and q are given by:

$$dF_{ext} = \left(-\frac{\varepsilon_0 A V_{DC}^2}{x_e^3} + K\right)dx + \frac{\varepsilon_0 A V_{DC}}{x_e^2} dV_{DC} \tag{9}$$

$$dq = -\frac{\varepsilon_0 A V_{DC}}{x_e^2} dx + \frac{\varepsilon_0 A}{x_e} dV_{DC} \tag{10}$$

For a given DC bias V_{DC}, the top electrode will move to the lowest-energy position, after which F_{ext} will be zero. If an additional AC voltage is applied to the transducer, the small signal may also influence the position of the top electrode. The small-signal AC voltage with angular frequency ω will induce two mechanical variables: a net force on the top electrode (F_{ext}) and a velocity of the top electrode (v); and two electrical variables: voltage on the top electrode (V) and current (i). Those four variables and their differential equations are expressed in eq. (11) and eq. (12). $\hat{F}$, $\hat{v}$, $\hat{V}$ and $\hat{\imath}$ are the amplitude of the oscillating force, velocity, voltage and current respectively.

$$F_{ext} = \hat{F}e^{j\omega t};\ v = \hat{v}e^{j\omega t};\ V = V_{DC} + \hat{V}e^{j\omega t};\ i = \hat{\imath}e^{j\omega t} \tag{11}$$

$$\frac{dF_{ext}}{dt} = j\omega\hat{F}e^{j\omega t};\ \frac{dx}{dt} = v = \hat{v}e^{j\omega t};\ \frac{dV}{dt} = j\omega\hat{V}e^{j\omega t};$$
$$\frac{dq}{dt} = i = i_0 e^{j\omega t} \tag{12}$$

According to the second axiom of Newton,

$$m\frac{dv}{dt} = -F_{ext} - \alpha v \tag{13}$$

Inserting eq. (12) into eq. (9), eq. (10) and eq. (13), we obtain the following equation system with four variables,

$$j\omega\hat{F} = \left(-\frac{\varepsilon_0 A V_{DC}^2}{x_e^3} + K\right)\hat{v} + \frac{\varepsilon_0 A V_{DC}}{x_e^2} j\omega\hat{V} \tag{14}$$

$$\hat{\imath} = -\frac{\varepsilon_0 A V_{DC}}{x_e^2}\hat{v} + \frac{\varepsilon_0 A}{x_e} j\omega\hat{V} \tag{15}$$

$$\hat{F} = -(j\omega m + \alpha)\hat{v} \tag{16}$$

By solving the equation system (14) to (16) above, the device impedance is found to follow [12]

$$Z_{up} = \frac{\hat{u}}{\hat{\imath}} = \frac{1}{j\omega C_p} * \frac{\omega^2 m - j\omega\alpha + \frac{\varepsilon_0 A_p V_{DC}^2}{x_e^3} - K}{\omega^2 m - j\omega\alpha - K} \tag{17}$$

It is clear from eq. (17) that the RF MEMS switch is far from purely parallel-plate capacitive, as usually assumed (and observed at radio-frequencies). The impedance shows a pole at $\omega^2 = K/m$. The impedances of the up-state switch at high frequency ($Z_{up,HF}, \omega^2 \gg K/m$) and low frequency ($Z_{up,LF}, \omega^2 \ll K/m$) follow from (17) are given by:

$$Z_{up,HF} = \frac{1}{j\omega C_p} * \frac{\omega^2 m}{\omega^2 m} = \frac{1}{j\omega} * \frac{x_e}{\varepsilon_0 A_p} = \frac{1}{j\omega C_p} \tag{18}$$

$$Z_{up,LF} = \frac{1}{j\omega C_p} * \frac{\frac{\varepsilon_0 A_p V_{DC}^2}{x_e^3} - K}{-K} = \frac{1}{j\omega C_p} * \left(1 - \frac{A_p \varepsilon_0 V_{DC}^2}{K x_e^3}\right) \tag{19}$$

Both limit cases are again purely capacitive, but the capacitance at low frequency is larger than the parallel-plate capacitance, as indeed experimentally observed (see figure 2). Moreover, the capacitance difference far from resonance is frequency independent, as indeed observed.

The DUT shows a significant mechanical resonance at 17 kHz at zero DC bias, as confirmed with Laser Doppler vibrometer measurements. When the frequency approaches this frequency, the real part of the impedance increases.

The correction term in eq. (19) can be directly calculated because K can be estimated from V_{pi} [12],

$$K = \frac{27\varepsilon_0 A_p V_{pi}^2}{8\left(x_0 - x_d - \frac{x_d}{\varepsilon_r}\right)^3} \tag{20}$$

Replotting the measurements in figure 2 at low and high frequencies to isolate the additional term in (19) yields a quantitative match between the observed and predicted capacitances, as shown in figure 4 - without any parameter fitting. Since the capacitance difference far from resonance is frequency independent, the up-state C_{LF} in figure 2 can represent capacitance at frequency below 10 Hz, and C_{HF} can represent the capacitance at frequency above 100 kHz. Because of limitations of our measurement equipment, the up-state capacitance (~0.5 pF) cannot be accurately measured between 10 Hz and 100 kHz.

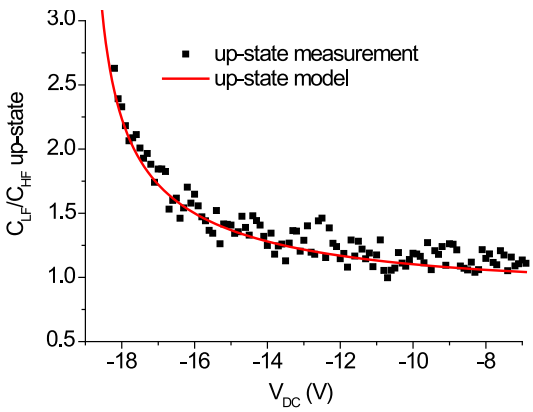

FIGURE 4. Measured and modeled up-state $C_{\text{LF}}/C_{\text{HF}}$ versus V_{DC}.

In short, we measured parallel-plate capacitance at HF which is determined by the DC bias; however, the top electrode displaces with AC voltage at LF and contributes to the measured AC current, resulting in an increase of measured capacitance.

V. DOWN-STATE CAPACITANCE

If we describe the down-state with the same one-dimensional model as the up-state, we must account for the additional

contact force exerted by the dielectric film. A primitive description of this situation would yield again equation (17) with a higher spring constant to account for this mechanical contact and a different damping factor. To complicate matters, all model parameters become strongly gap and (therefore) voltage dependent.

The associated down-state first resonance frequency is in the few-MHz range for the device under study, as established by a 3D FEM calculation [13]. This explains the observed (small) difference between HF and RF capacitance in the down-state. The one-dimensional model leading to equation (17) however cannot explain the observed differences between LF and HF in the down-state.

To explain these, it is necessary to take into account that neither top electrode nor dielectric are perfectly flat. In the down-state, the movement of the top electrode is constrained by the points of contact to the dielectric on the bottom electrode. Away from those points of contact, air gaps remain under the top electrode – in particular near the springs. Parts of the top electrode may therefore still move upon an electrostatic force, contributing to the AC current, and changes of measured capacitance. This is visible in a vibrometer, as shown in the inset of figure 5.

At atmospheric pressure, the top electrode movement is hampered by the squeeze film effect [14]. Mechanical motion of the top electrode compresses the partially enclosed gas volume between the electrodes. Given enough time, this pressure change leads to a lateral gas flow. As a consequence, this leads to viscous damping at very low frequencies, and an additional spring force (squeeze film stiffness) at higher frequencies. The FEM model mentioned earlier [13] predicts a transition around 5 kHz for this effect.

Intuitively, one can argue that this effect should be most prominent when the applied field is low. Near pull-out, the top electrode is close to releasing. Therefore, the top electrode is relatively free to move and the gas volume between the electrodes may be significant. With the decrease of frequency, the top electrode movement gradually appears while gas compression decreases, resulting in an increase of the measured capacitance near pull-out, as shown in figure 5.

The squeeze film effect is significantly reduced if the MEMS switch is operated in vacuum. As a result, much higher vibration amplitudes are observed near pull-out (DC bias of 12 V) in vacuum, as shown in figure 6 (a). In the vibrometer measurement, we measure the vibration amplitude of an array of positions across the top electrode. The y-axis 'displacement' in figure 6 is the average vibration amplitude of all positions. When the DC bias is far from V_{po}, the top electrode hardly displaces in both atmospheric pressure and vacuum because of the limited space between top electrode and the dielectric layer on bottom electrode. Thus, at DC bias of 25 V, the vibration amplitude is close to zero under both vacuum and atmospheric pressure. As shown in figure 6 (b), the vibration amplitudes in vacuum significantly increase when the DC bias is approaching pull-out, whereas the vibration amplitude under atmospheric pressure remains low at the down-state.

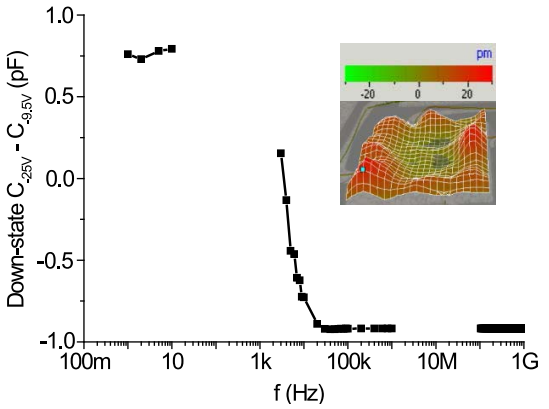

FIGURE 5. **The difference between down-state capacitance at -25 V (C_{-25V}) and -9.5 V ($C_{-9.5V}$) as a function of frequency. The inset shows the vibration amplitude of the top electrode in down-state measured at reduced pressure (<3×10^{-4} mbar) at 1.5 MHz.**

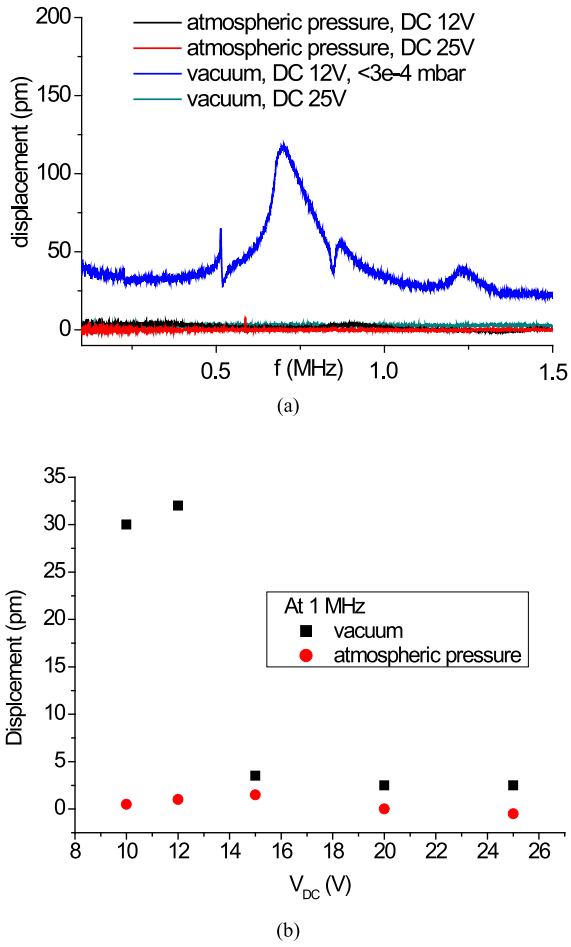

FIGURE 6. **Vibrometer measurement in atmospheric and low pressure: (a) displacement-frequency relation at DC bias of 12 V and 25 V; (b) displacement-V_{DC} relation at 1 MHz.**

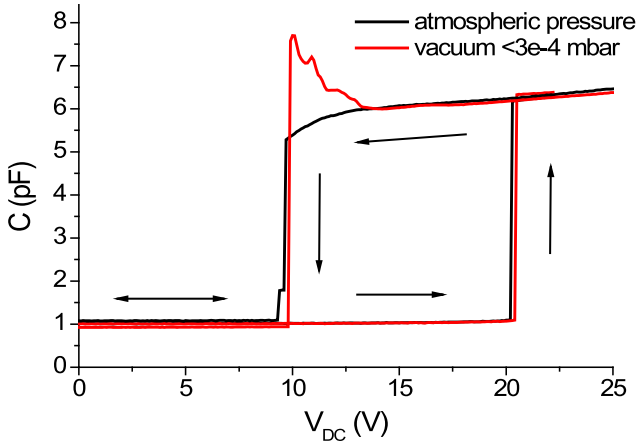

FIGURE 7. HF *C-V* curve at 100 kHz at atmospheric and low pressure. The setup used to this purpose did not allow for de-embedding, leading to a slightly higher overall capacitance compared to figure 2.

To further confirm the role of squeeze film damping, we carried out a high-frequency *C-V* measurement in a vacuum chamber, see figure 7. The high-frequency, low-pressure result shows a similar capacitance behavior in the down-state as the LF capacitance under atmospheric pressure (see figure 2).

In the down-state, each device will behave differently because of microscopic physical differences. This leads to a large device-to-device spread in the LF capacitance close to pull-out (figure 3 (a)). This spread is expected to occur also for low-pressure measurements at higher frequency (>100 kHz). The down-state capacitance near pull-out is therefore not well controlled and this operating condition should be avoided.

VI. CONCLUSION

The small-signal impedance of an RF MEMS capacitive switch was studied across 11 orders of magnitude in frequency. Most of the *C-V* curve of the switch is almost frequency independent across the full frequency range. However, the low-frequency capacitance (<10 Hz) is up to 200% higher around the pull-in voltage and 25% higher around the pull-out voltage than the high-frequency capacitance (>100 kHz). In the up-state, this can be attributed to the mechanical movement of the top electrode at low frequencies. A one-dimensional spring-mass model quantitatively reproduces the up-state behavior. The difference between LF and HF capacitance in the down-state is attributed to squeeze-film effects in the residual gas volume between the top electrode and the dielectric film. This assumption is supported by vibrometer measurements, FEM simulations, and *C-V* measurements at reduced pressure. The low frequency capacitance measurement detects the coupling between mechanical and electrical operation of RF MEMS switches, and helps to construct a comprehensive understanding of the device. A concise impedance model for the RF MEMS capacitive switch should include these properties, in particular for biasing voltages close to pull-in and pull-out.

REFERENCES

[1] P. Gammel, G. Fischer, and J. Bouchaud, "RF MEMS and NEMS technology, devices, and applications," *Bell Labs Tech. J.*, vol. 10, no. 3, pp. 29–59, 2005, doi: 10.1002/bltj.20103.
[2] G. M. Rebeiz, *RF MEMS: Theory, Design, and Technology*. Hoboken, NJ, USA: Wiley, 2003, doi: 10.1002/0471225282.
[3] J. Iannacci, *Practical Guide to RF-MEMS*. Weinheim, Germany: Wiley, 2013, doi: 10.1002/9783527680856.
[4] G. M. Rebeiz, "RF MEMS switches: Status of the technology," in *Proc. Int. Conf. Solid State Sens. Actuators Microsyst.*, Boston, MA, USA, 2003, pp. 1726–1729, doi: 10.1109/SENSOR.2003.1217118.
[5] R. W. Herfst, P. G. Steeneken, M. P. J. Tiggelman, J. Stulemeijer, and J. Schmitz, "Fast RF-CV characterization through high-speed 1-port S-parameter measurements," *IEEE Trans. Semicond. Manuf.*, vol. 25, no. 3, pp. 310–316, 201, doi: 10.1109/TSM.2012.2202752.
[6] G. Li *et al.*, "Investigation of charge injection and relaxation in multilayer dielectric stacks for capacitive RF MEMS switch application,"*IEEE Trans. Electron Devices*, vol. 60, no. 7, pp. 2379–2387, Jul. 2013, doi: 10.1109/TED.2013.2263252.
[7] H.-H. Yang, H. Zareie, and G. M. Rebeiz, "A high power stress-gradient resilient RF MEMS capacitive switch," *IEEE J. Microelectromech. Syst.*, vol. 24, no. 3, pp. 599–607, Jun. 2015, doi: 10.1109/JMEMS.2014.2335173.
[8] A. Persano, F. Quaranta, M. C. Martucci, P. Siciliano, and A. Cola, "On the electrostatic actuation of capacitive RF MEMS switches on GaAs substrate," *Sens. Actuators A Phys.*, vol. 232, pp. 202–207, Aug. 2015, doi: 10.1016/j.sna.2015.05.008.
[9] C. Ryan *et al.*, "Identification of the transient stress-induced leakage current in silicon dioxide films for use in microelectromechanical systems capacitive switches," *Appl. Phys. Lett.*, vol. 106, no. 17, 2015, Art. no. 172904, doi: 10.1063/1.4919718.
[10] J. Wang, C. Salm, and J. Schmitz, "Comparison of C-V measurement methods for RF-MEMS capacitive switches," in *Proc. IEEE Conf. Microelect. Test Struct.*, Osaka, Japan, 2013, pp. 53–58, doi: 10.1109/ICMTS.2013.6528145.
[11] "Performing very low frequency capacitance-voltage measurements on high impedance devices using the model 4200-SCS semiconductor characterization system," Keithley application note series. [Online]. Available: http://www.tek.com/sites/tek.com/files/media/document/resources/VLF_CV_AppNote.pdf
[12] M. Elwenspoek, G. Krijnen, R. Wiegerink, and T. Lammering, *Introduction to Mechanics and Transducer Science*. Enschede, The Netherlands: Univ. Twente.
[13] J. Bielen, J. Stulemeijer, D. Ganjoo, D. Ostergaard, and S. Noijen, "Fluid-electrostatic-mechanical modeling of the dynamic response of RF-MEMS capacitive switches," in *Proc. EuroSimE Conf.*, 2008, pp. 1–8, doi: 10.1109/ESIME.2008.4525083.
[14] M. Bao and H. Yang, "Squeeze film air damping in MEMS," *Sens. Actuators A Phys.*, vol. 136, no. 1, pp. 3–27, 2007, doi: 10.1016/j.sna.2007.01.008.

JIAHUI WANG received the B.Sc and M.Sc. degrees from the Electronical Engineering Department, Wuhan National Laboratory for Optoelectronics, Huazhong University of Science and Technology, Wuhan, China, in 2008 and 2011, respectively. She is currently pursuing the Ph.D. degree with the University of Twente, Enschede, The Netherlands. Her research interest includes fabrication and reliability on novel materials, devices or MEMS.

JEROEN BIELEN received the M.Sc. degree in electrical engineering and the Registered Technological Designer degree (cum laude) in microsystem technology from Twente University in 1994 and 1997, respectively. After 4 years clean room experience in MESA+, since 1998, he has been a Principal Reliability Engineer with Philips Semiconductors (currently NXP) on thermal analysis (characterization, finite element modeling, and design) and on reliability statistics and the physics of failure-based prediction of package related failure mechanisms and risk mitigation strategies. In 2005, he joined the NXP RF-MEMS Program (successively transferred to Epcos and TDK) as a Device Designer. He authored or coauthored over 30 journal and conference papers and holds two patents. His current interest is electro-mechanical modeling and device physics of acoustic wave resonators and reliability modeling of heterogeneous integrated RF systems (PAMiD modules).

CORA SALM (M'98) received the Ph.D. degree from the University of Twente, Enschede, The Netherland, in 1997. Her current research interests include micro- and nano-device and systems reliability.

GIJS KRIJNEN received the Ph.D. (cum laude) degree from the University of Twente. He currently is with the Robotics and Mechatronics Group of the University of Twente. He has (co-) authored over 100 refereed journal papers, ten book chapters, and 235 conference contributions on a variety of subjects including nonlinear integrated optics, micro-mechanical sensors and actuators, biomimetic flow and inertial sensors, and parametric and nonlinear transduction. His interests are in Lifelike (MEMS) transducers in general, bio-mimetic flow-sensors in particular, parametric sensing schemes, and additive manufacturing. He has been a fellow of the Royal Netherlands Academy of Arts and Sciences and was a recipient of VICI grant by The Netherlands Organisation for Scientific Research in 2005 for research on Lifelike flow-sensors (BioEARS).

JURRIAAN SCHMITZ (M'02–SM'05) received the M.Sc. (Hons.) and Ph.D. degrees in experimental physics from the University of Amsterdam, Amsterdam, The Netherlands, in 1990 and 1994, respectively.

He joined Philips Research, Eindhoven, The Netherlands, in 1994, as the Senior Scientist. In 2002, he left Philips to become a Professor of Semiconductor Components with the University of Twente, Enschede, The Netherlands.